Saturation of 640-nm absorption in Cr^{4+}:YAG for an InGaN laser diode pumped passively Q-switched Pr^{3+}:YLF laser

Hiroki Tanaka, Ryosuke Kariyama, Kodai Iijima, Kenichi Hirosawa and Fumihiko Kannari*

Department of Electronics and Electrical Engineering, Keio University, 3-14-1, Hiyoshi, Kohoku-ku, Yokohama 223-8522, Japan

*kannari@elec.keio.ac.jp

Abstract: We measure the absorption recovery time, the ground- and excited-state absorption cross sections of a Cr^{4+}:YAG crystal at 640 nm for the first time. A pump-probe measurement reveals the existence of two recovery times of 26 ns and 5.6 μs. By a Z-scan experiment, the ground- and excited-state absorption cross sections are estimated to be $1.70-1.75\times10^{-17}$ and $0.95-1.00\times10^{-17}$cm^2, respectively. The adequacy of the proposed model and the accuracy of the estimated parameters of the saturable absorber are verified by reproducing the experimentally obtained performance of a passively Q-switched Pr^{3+}:YLF laser with the Cr^{4+}:YAG saturable absorber from rate equation analysis.

OCIS codes: (140.3380) Laser materials; (140.7300) Visible lasers; (140.3580) Lasers, solid-state; (140.3480) Lasers, diode-pumped; (140.3540) Lasers, Q-switched.

References and links

1. A. Richter, E. Heumann, G. Huber, V. Ostroumov, and W. Seelert, "Power scaling of semiconductor laser pumped Praseodymium-lasers," Opt. Express **15**, 5172–5178 (2007).
2. A. Richter, N. Pavel, E. Heumann, G. Huber, D. Parisi, A. Toncelli, M. Tonelli, A. Diening, and W. Seelert, "Continuous-wave ultraviolet generation at 320 nm by intracavity frequency doubling of red-emitting Praseodymium lasers," Opt. Express **14**, 3282–3287 (2006).
3. K. Hashimoto and F. Kannari, "High-power GaN diode-pumped continuous wave Pr^{3+}-doped $LiYF_4$ laser," Opt. Lett. **32**, 2493–2495 (2007).
4. T. Gün, P. Metz, and G. Huber, "Power scaling of laser diode pumped Pr^{3+}:$LiYF_4$ cw lasers: efficient laser operation at 522.6 nm, 545.9 nm, 607.2 nm, and 639.5 nm," Opt. Lett. **36**, 1002–1004 (2011).
5. T. Gün, P. Metz, and G. Huber, "Efficient continuous wave deep ultraviolet Pr^{3+}:$LiYF_4$ laser at 261.3 nm," Appl. Phys. Lett. **99**, 181103 (2011).
6. P. W. Metz, F. Reichert, F. Moglia, S. Müller, D.-T. Marzahl, C. Kränkel, and G. Huber, "High-power red, orange, and green Pr^{3+}:$LiYF_4$ lasers," Opt. Lett. **39**, 3193–3196 (2014).
7. P. W. Metz, K. Hasse, D. Parisi, N.-O. Hansen, C. Krnkel, M. Tonelli, and G. Huber, "Continuous-wave Pr^{3+}:BaY_2F_8 and Pr^{3+}:$LiYF_4$ lasers in the cyan-blue spectral region," Opt. Lett. **39**, 5158–5161 (2014).
8. Z. Liu, Z. Cai, B. Xu, S. Huang, C. Zeng, Y. Yan, F. Wang, H. Xu, J. Doualan, P. Camy, and R. Moncorgé, "Continuous-Wave Laser Emission of Pr:$LiYF_4$ at 695.8 nm," IEEE J. Quantum Electron. **26**, 675–677 (2014).
9. J. Kojou, R. Abe, R. Kariyama, H. Tanaka, A. Sakurai, and F. Kannari, "InGaN diode pumped actively Q -switched intracavity frequency doubling Pr:$LiYF_4$ 261 nm laser," Appl. Opt. **53**, 2030–2036 (2014).
10. R. Abe, J. Kojou, K. Masuda, and F. Kannari, "Cr^{4+}-Doped $Y_3Al_5O_{12}$ as a Saturable Absorber for a Q-Switched and Mode-Locked 639-nm Pr^{3+}-Doped $LiYF_4$ Laser," Appl. Phys. Express **6**, 032703 (2013).
11. H. Okamoto, K. Kasuga, I. Hara, and Y. Kubota, "Visible-NIR tunable Pr^{3+}-doped fiber laser pumped by a GaN laser diode," Opt. Express **17**, 20227–20232 (2009).

#240833 Received 15 May 2015; revised 30 Jun 2015; accepted 3 Jul 2015; published 17 Jul 2015

12. Y. Fujimoto, J. Nakanishi, T. Yamada, O. Ishii, and M. Yamazaki, "Visible fiber lasers excited by GaN laser diodes," Prog. Quantum Electron. **37**, 185–214 (2013).
13. D.-T. Marzahl, F. Reichert, B. Stumpf, P. W. Metz, C. Kränkel, and G. Huber, "Spectroscopic Properties and Laser Operation of Sm,Mg:$SrAl_{12}O_{19}$," in CLEO: 2014, OSA Technical Digest (online) (Optical Society of America, 2014), paper SM3F.2.
14. G. Bolognesi, D. Parisi, D. Calonico, G. A. Costanzo, F. Levi, P. W. Metz, C. Kränkel, G. Huber, and M. Tonelli, "Yellow laser performance of Dy^{3+} in co-doped Dy,Tb:$LiLuF_4$," Opt. Lett. **39**, 6628–6631 (2014).
15. F. Reichert, F. Moglia, P. W. Metz, A. Arcangeli, D. Marzahl, S. Veronesi, D. Parisi, M. Fechner, M. Tonelli, and G. Huber, "Prospects of Holmium-doped fluorides as gain media for visible solid state lasers," Opt. Mater. Express **5**, 88–101 (2015).
16. R. Feldman, Y. Shimony, and Z. Burshtein, "Dynamics of chromium ion valence transformations in Cr,Ca:YAG crystals used as laser gain and passive Q-switching media," Opt. Mater. **24**, 333–344 (2003).
17. H. Eilers, K. R. Hoffman, W. M. Dennis, S. M. Jacobsen, and W. M. Yen, "Saturation of 1.064 μm absorption in Cr,Ca:$Y_3Al_5O_{12}$ crystals," Appl. Phys. Lett. **61**, 2958–2960 (1992).
18. H. Eilers, U. Hömmerich, S. M. Jacobsen, W. M. Yen, K. R. Hoffman, and W. Jia, "Spectroscopy and dynamics of Cr^{4+}:$Y_3Al_5O_{12}$," Phys. Rev. B **49**, 15505–15513 (1994).
19. Y. Shimony, Z. Burshtein, and Y. Kalisky, "Cr^{4+}:YAG as Passive Q-switch and Brewster Plate in a Pulsed Nd:YAG laser," IEEE J. Quantum Electron. **31**, 1738–1741 (1995).
20. G. Xiao, J. H. Lim, S. Yang, E. Van Stryland, M. Bass, and L. Weichman, "Z-scan measurement of the ground and excited state absorption cross sections of Cr^{4+} in yttrium aluminum garnet," IEEE J. Quantum Electron. **35**, 1086–1091 (1999).
21. A. Okhrimchuk and A. Shestakov, "Absorption saturation mechanism for YAG:Cr^{4+} crystals," Phys. Rev. B **61**, 988–995 (2000).
22. H. Ridderbusch and T. Graf, "Absorption in Cr^{4+}:YAG Crystals," IEEE J. Quantum Electron. **43**, 168–173 (2007).
23. V. V. Zelenogorskii and E. A. Khazanov, "Influence of the photoelastic effect on the thermal lens in a YLF crystal," Quantum Electron. **40**, 40–44 (2010).
24. A. Richter, *Laser Parameters and Performance of Pr^{3+}-Doped Fluorides Operating in the Visible Spectral Region* (Cuvillier Verlag, 2008), Chap. 3.

1. Introduction

In the last decade, efficient solid-state lasers that oscillate directly in the visible spectral region have been developed. Up to now, laser actions in the visible region have been demonstrated with several gain media, including tetravalent praseodymium (Pr^{3+})- [1–12], samarium (Sm^{3+})- [13], dysprosium (Dy^{3+})- [12, 14], and holmium (Ho^{3+})-doped materials [15]. Currently, the most efficient lasing in the visible region is achieved with Pr^{3+}-doped fluoride materials, such as lithium yttrium tetra-fluoride ($LiYF_4$: YLF) crystal, and ZBLAN [11] and AlF_3 glass fibers [12]. In addition to their efficiency, the laser media are attractive because they have multiple laser lines in the visible spectral region, which correspond to the colors of cyan (~480 nm), green (~520 nm), orange (~610 nm), red (~640 nm) and deep-red (~700 and 720 nm). Laser oscillation in all of these laser lines has already been achieved [1–7], mainly owing to the development of efficient pump sources for Pr^{3+}. Pr^{3+} has its absorption peaks around 440 nm and 480 nm, and these peaks became available by the development of the InGaN blue laser diode (LD) and frequency doubled optically pumped semiconductor laser (2ω-OPSL). Pr^{3+} had previously been pumped by argon (Ar)-ion laser.

The first Pr^{3+}:YLF laser with 2ω-OPSL was achieved by Richter *et al*. They demonstrated efficient red and green lasers [1], and a CW intra-cavity second harmonic generation (SHG) at 320 nm [2]. Hashimoto *et al.* presented a red Pr^{3+}:YLF laser with a high-power InGaN blue LD pumping [3]. Gün *et al.* performed CW laser oscillation at 522.6, 545.9, 607.2, and 639.5 nm with a pair of blue LDs as the pump source [4], and they extended the visible laser to 261-nm CW UV laser by intra-cavity SHG [5]. Recently, Metz *et al.* successfully demonstrated the power scaling of red, orange, and green Pr^{3+}:YLF lasers by utilizing a 2ω-OPSL that delivered 5-W output power at 479 nm as the pump source [6]. Maximum output powers reached 2.8, 1.8 and 2.9 W, and slope efficiencies of 68, 48 and 72% were recorded for 640-, 607-, and 523-nm

#240833 Received 15 May 2015; revised 30 Jun 2015; accepted 3 Jul 2015; published 17 Jul 2015

oscillations, respectively. The optical-optical efficiency of 2ω-OPSL pumped Pr^{3+}:YLF laser is better than that pumped by blue LD since the worse beam quality of the blue LD results in lower mode-matching efficiencies.

Kojou *et al.* performed an active Q-switching of Pr^{3+}:YLF laser pumped by an InGaN-LD of 3.5-W output power, and its intra-cavity SHG using the high peak power of Q-switched pulses. At the wavelengths of 261 and 320 nm, the maximum peak powers of 61.6 and 594 W were achieved, respectively. The study examined the Q-switched Pr^{3+}:YLF laser performance with rate equations for the first time [9].

The tetravalent chromium (Cr^{4+})-doped yttrium aluminum garnet (YAG) crystal has been known as the typical saturable absorber for Q-switching of neodymium (Nd) lasers such as Nd:YAG and Nd:YVO_4 lasers, which oscillate around a wavelength of 1 μm. The saturable absorber is suitable for high-power Q-switched laser owing to the high thermal conductivity of the YAG crystal which leads to increase its damage threshold. Many research groups have been working with the saturable absorber, and Q-switched Nd lasers of high averaged power, microchip laser, and Q-switched mode-locking have been demonstrated. However, the saturable absorption of Cr^{4+}:YAG in the visible region hadn't been recognized before the recent work of Abe *et al.* [10], despite Feldman *et al.* having already observed a strong absorption around the red wavelength, which corresponds to the transition of the tetrahedral Cr^{4+}, $^3B_1(^3A_2) \rightarrow ^3A_2(^3T_1)$ [16]. Abe *et al.* showed that the Cr^{4+}:YAG crystal can also behave as a saturable absorber in the visible region by demonstrating the passive Q-switching and Q-switched mode-locking of Pr^{3+}:YLF laser with the Cr^{4+}:YAG saturable absorber [10]. At the wavelength of 1 μm, the Cr^{4+}:YAG saturable absorber has been deeply investigated, and its recovery time, ground-state and excited state absorption cross sections are now available [16–21]. However, these important parameters in the visible region haven't been investigated.

In this paper, we estimate the key parameters of the Cr^{4+}:YAG crystal, which determine its saturable absorption action, absorption recovery time, and the ground-state and excited-state absorption cross sections; and we propose an effective model of the saturable absorber at 640 nm. Moreover, we demonstrate the passive Q-switching of a double high-power blue InGaN LD pumped Pr^{3+}:YLF red laser by employing the Cr^{4+}:YAG as the saturable absorber. The accuracy of the estimated parameters is verified by the fact that a rate equation analysis based on the estimated parameters reproduces the experimental laser performance. By simulating with the proposed model of the saturable absorber and the established rate equation model, we can further design a passive Q-switching microchip laser, and the calculated result shows that the pulse width of 860 ps, pulse energy of 11.5 μJ, and peak power of 13 kW are feasible.

2. Characterization of Cr^{4+}:YAG saturable absorber at wavelength of 640 nm

In this section, measurements for revealing parameters of a Cr^{4+}:YAG crystal are presented. In general, a slow saturable absorber can be modeled by the conventional four-level system shown in Fig. 1. The system has two absorption paths, from the ground-state E_1 to E_3 and from the excited-state E_2 to E_4. These absorptions are represented by the ground-state absorption cross section σ_{gs}, and excited-state absorption cross section σ_{es}. The temporal decay from the excited-state to the ground-state is characterized by its lifetime τ with the transition rate of $\exp(-t/\tau)$. In this model, the lifetimes of the levels E_3 and E_4 are assumed to be very fast so that the excited-state absorption cannot saturate. Therefore, the excited-state absorption represents the non-saturable loss of a saturable absorber. Once these three parameters, the ground- and excited-state absorption cross sections and the recovery time are revealed, the dynamics of the saturable absorber can be perfectly described. Many researchers have tried to evaluate these parameters at 1,064-nm wavelength [16–21]. However, reported values of the ground- and excited-state absorption cross sections were widely varied, while the recovery time has

#240833 Received 15 May 2015; revised 30 Jun 2015; accepted 3 Jul 2015; published 17 Jul 2015

been settled to be on the order of microseconds (3.5-4.1 μs) at room temperature. It should be noted that, although the reported cross sections differed greatly, the ratios σ_{gs}/σ_{es} were converged around 3.2-4.7.

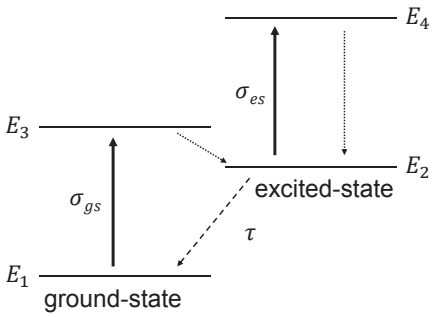

Fig. 1. Conventional four-level system representing a slow saturable absorber.

2.1. *Examination of absorption recovery time*

The characterization of Cr^{4+}:YAG saturable absorber started with the measurement of its absorption recovery time by means of the pump-probe experiment. The schematic view of the measurement is depicted in Fig. 2. We employed a pump laser with an actively Q-switched Pr^{3+}:YLF laser at wavelength of 640 nm, with pulse repetition frequency of 5 kHz, pulse width of 30 ns at full width at half maximum (FWHM), and pulse energy of around 10 nJ. The pump spot radius was measured to be 11 μm. As the probe laser, 10-mW continuous-wave (CW) LD of the same wavelength was used. These lasers were aligned so that two laser beams were overlapped within a Cr^{4+}:YAG 1.3-mm thick. The Cr^{4+}:YAG crystal was cut parallel to the < 100 > plane. The transmitted probe laser was detected by a photodiode (PD) (Hamamatsu, Si PIN photodiode S3883) and recorded by an oscilloscope (LeCroy WaveRunner 62Xi). When the pump pulse passed through the Cr^{4+}:YAG, the transmission rate of the irradiated area increased owing to its saturable absorption, and simultaneously, the transmission rate of the probe beam was also increased. After the pump pulse passed away, the bleached area would recover to its initial state with the characteristic lifetime. Hence, by recording the transient decay of the probe laser, the recovery time can be evaluated. The transient PD voltage recorded over 20 μs is shown as the solid line in Fig. 3(a). At a glance, the gradual decay indicates that the recovery time is several microseconds. The solid line in Fig. 3(b) is the PD voltage enlarged up to 200 ns. The normalized waveform of the pump pulse is shown as a solid blue line.

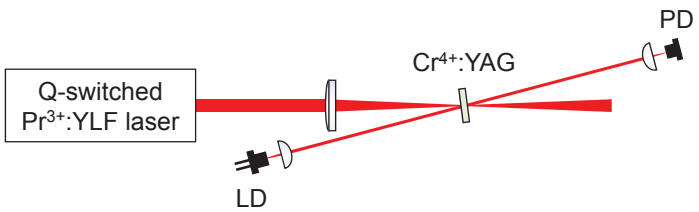

Fig. 2. Schematic view of pump-probe experiment to examine recovery time of Cr^{4+}:YAG saturable absorber.

#240833 Received 15 May 2015; revised 30 Jun 2015; accepted 3 Jul 2015; published 17 Jul 2015

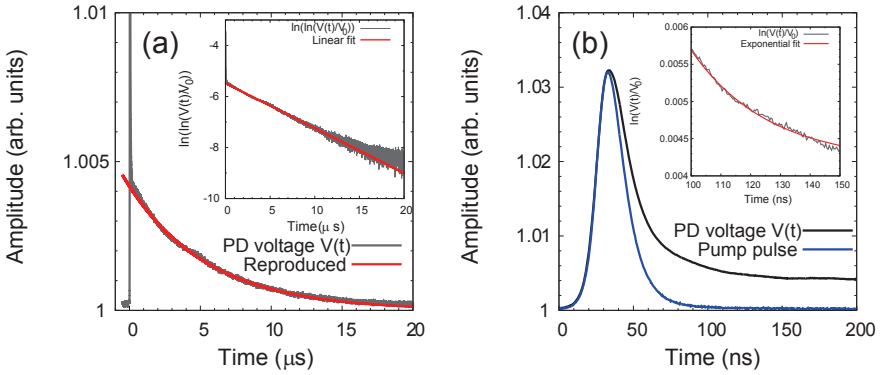

Fig. 3. (a) PD voltage recorded over 20 μs. The inset is an analysis of the longer recovery time. (b) PD voltage enlarged up to 200 ns. The inset is an analysis of the shorter recovery time.

Although the end-to-end width of the pump pulse was approximately 100 ns, there is a longer tail after the pump pulse has disappeared. Hence, this long tail told us of the existence of another shorter recovery time. We found out that the Cr^{4+}:YAG saturable absorber has two different recovery times at wavelength of 640 nm, while the saturation at 1,064 nm is determined by one characteristic lifetime. Therefore, the conventional model depicted in Fig. 1 is no longer suitable as the model for a wavelength of 640 nm, and the four-level system had to be modified so that it has two recovery times. It was straightforward to come up with the modified six-level system depicted in Fig. 4. This proposed model has two separate excited-states (E_2 and E_5), and their lifetimes are τ_1 and τ_2 ($\tau_1 < \tau_2$), respectively. The transition ratio from E_3 to E_2 is γ ($\gamma < 1$), and that to E_5 is $1-\gamma$. The excited-state absorption cross section of two excited-states was assumed to be identical. Please note that this six-level system is an equivalent model to describe the two absorption recovery time constants. Presumably deeper discussion would be required to describe the state E_5 to which only a trace of energy flows from E_3. We quantitatively estimated the two recovery times based on the proposed six-level model. The temporal transmission of the saturable absorber $T(t)$ after irradiation by a pump pulse is described by the

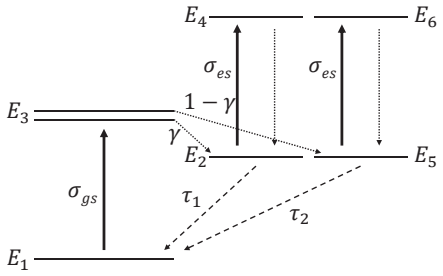

Fig. 4. Proposed six-level model for Cr^{4+}:YAG saturable absorber at 640 nm.

#240833 Received 15 May 2015; revised 30 Jun 2015; accepted 3 Jul 2015; published 17 Jul 2015

following equation.

$$T(t) = \exp\left[\left\{-\sigma_{gs}\left(n_{tot} - n_{es}^{(1)}(0)\exp\left(-\frac{t}{\tau_1}\right) - n_{es}^{(2)}(0)\exp\left(-\frac{t}{\tau_2}\right)\right)\right.\right.$$
$$\left.\left.-\sigma_{es}\left(n_{es}^{(1)}(0)\exp\left(-\frac{t}{\tau_1}\right) + n_{es}^{(2)}(0)\exp\left(-\frac{t}{\tau_2}\right)\right)\right\} l_{SA}\right]. \quad (1)$$

Here, n_{tot} is the total density of Cr^{4+} that contributes to the absorption, $n_{es}^{(1)}(0)$ and $n_{es}^{(2)}(0)$ are the densities of Cr^{4+} in the first excited-state (E_2 in Fig. 4) and the second excited-state (E_5 in Fig. 4) just after the incidence of a pump pulse, respectively. l_{SA} is the thickness of the Cr^{4+}:YAG crystal. In the case where $t \gg \tau_1$, the terms including $\exp(-t/\tau_1)$ can be considered to be zero, and therefore, Eq. (1) can be simplified to Eq. (2):

$$T(t) = \exp\left[\left\{-\sigma_{gs}\left(n_{tot} - n_{es}^{(2)}(0)\exp\left(-\frac{t}{\tau_2}\right)\right) - \sigma_{es}\left(n_{es}^{(2)}(0)\exp\left(-\frac{t}{\tau_2}\right)\right)\right\} l_{SA}\right]. \quad (2)$$

Furthermore, the Eq. (2) can be reduced to the following equation:

$$\ln\left(\ln\left(\frac{T(t)}{T_0}\right)\right) = -\frac{t}{\tau_2} + \ln\left(\ln\left(\frac{T(0)}{T_0}\right)\right). \quad (3)$$

An initial transmittance of a saturable absorber T_0 is theoretically given by the following equation:

$$T_0 = \exp\left(-\sigma_{gs} n_{tot} l_{SA}\right). \quad (4)$$

According to Eq. (3), the longer recovery time τ_2 can be obtained from the slope of $\ln(\ln(V(t)/V_0))$, which provides a linear line, where V is the recorded PD voltage, and V_0 is that corresponds to the initial transmission T_0. The inset in Fig. 3(a) is the plot of $\ln(\ln(V(t)/V_0))$ directly calculated from the experimentally recorded PD voltage, and the longer recovery time τ_2 was estimated to be 5.6 μs as its slope. The reproduced fitting curve calculated from the estimated recovery time is shown as the red solid-line in Fig. 3(a), and it shows perfect agreement with the experimental curve.

On the other hand, in the case, where $t \ll \tau_2$, the terms including $\exp(-t/\tau_2)$ in Eq. (1) can be considered to be unity, and we obtained Eq. (5):

$$T(t) = \exp\left[\left\{-\sigma_{gs}\left(n_{tot} - n_{es}^{(1)}(0)\exp\left(-\frac{t}{\tau_1}\right) - n_{es}^{(2)}(0)\right)\right.\right.$$
$$\left.\left.-\sigma_{es}\left(n_{es}^{(1)}(0)\exp\left(-\frac{t}{\tau_1}\right) + n_{es}^{(2)}(0)\right)\right\} l_{SA}\right]. \quad (5)$$

Then, by dividing Eq. (5) by the initial transmission rate T_0, and by taking a logarithm, Eq. (5) is transformed into Eq. (6):

$$\ln\left(\frac{T(t)}{T_0}\right) = \left(\sigma_{gs} - \sigma_{es}\right) n_{es}^{(1)}(0) l_{SA} \exp\left(-\frac{t}{\tau_1}\right) + \left(\sigma_{gs} - \sigma_{es}\right) n_{es}^{(2)}(0) l_{SA}. \quad (6)$$

This equation tells us that the curve of $\ln(V(t)/V_0)$ has the form of $C_1\exp(-t/\tau_1) + C_2$ when the decay from the second excited-state is negligible, where C_1 and C_2 are constants. The inset of Fig. 3(b) is the plot of $\ln(V(t)/V_0)$ calculated from the experimental curve. Again, because the end-to-end pulse width of the employed pump pulse was shorter than 100 ns, the equation was applied after the pump pulse had terminated. Within the time range, from 100 ns to 200 ns, the

#240833 Received 15 May 2015; revised 30 Jun 2015; accepted 3 Jul 2015; published 17 Jul 2015

decay from the second excited-state is negligible as the lifetime of that state was estimated to be 5.6 μs. The shorter recovery time τ_1 was evaluated by fitting an exponential decay to the inset of Fig. 3(b), and it showed the best fit with a recovery time of 26 ns as shown by the blue line in the figure. The transition ratio γ (see Fig. 4) is evaluated from the experimental performance of the passively Q-switched laser as described in section 3.

2.2. Examination of ground- and excited-state absorption cross sections

In this section, we perform the evaluation of the absorption cross sections of a Cr^{4+}:YAG saturable absorber at 640 nm by Z-scan technique. The schematic view of the measurement is depicted in Fig. 5.

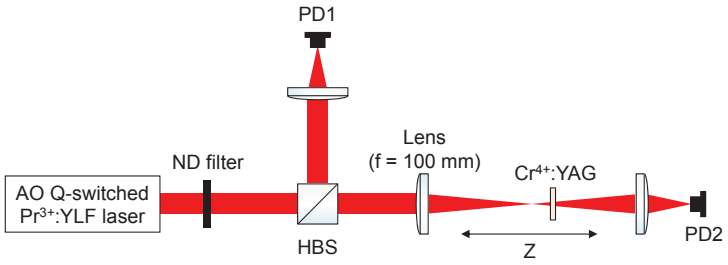

Fig. 5. Schematic view of Z-scan measurement.

We again employed an actively Q-switched Pr^{3+}:YLF laser at 640 nm with pulse repetition frequency of 5 kHz and pulse width of 15 ns (FWHM). Its beam was nearly fundamental mode ($M^2 < 1.1$). A pump beam was split into two beam paths by a half beam splitter (HBS). One of the split beams was directly detected by a photodiode (PD1), and the other was focused into a Cr^{4+}:YAG crystal by a lens of 100-mm focal length, and subsequently, the transmitted beam was detected by another photodiode (PD2). By using a CMOS image sensor, the spot of the pump beam was confirmed to be symmetric and its radius was measured to be 23 μ*m*. The transmittance of the Cr^{4+}:YAG crystal was obtained as the fraction of energy of the transmitted pulse compared with the energy of pulse detected by PD1. Note that the linearlity of pulse energies detected by PD1 and PD2 was confirmed before the measurement. The transmittance was recorded for each position of the Cr^{4+}:YAG along the optical axis (Z-axis). The absorption cross sections were estimated by reproducing the experimental Z-scan curve (plots of transmittance of the saturable absorber with respect to its position around the focal spot) by numerical simulation based on rate equations. Xiao *et al.* performed estimation of absorption cross sections of Cr^{4+}:YAG at a wavelength of 1,064 nm using the technique, and they mentioned the necessity of Z-scan curves with at least two different pump pulse energies [20]. In fact, there are infinite pairs of ground- and excited-state absorption cross sections to fit a single Z-scan curve. However, a pair of cross sections can be determined by reproducing Z-scan curves with different pulse energies. In our experiment, we employed 1.3- and 2.4-mm-thick Cr^{4+}:YAG crystals (Scientific Materials Inc.), and their end faces were both anti-reflection (AR) coated. Their initial transmittances were 94.6 and 91.7%, respectively. Z-scan curves with Cr^{4+}:YAG crystals of different thicknesses are shown in Fig. 6. For each crystal, measurements were performed with different pulse energies. For the measurements with the 1.3-mm crystal, pulse energies were set to 0.60 and 6.0 μJ, and 0.59 and 5.5 μJ for the 2.4-mm crystal.

#240833 Received 15 May 2015; revised 30 Jun 2015; accepted 3 Jul 2015; published 17 Jul 2015

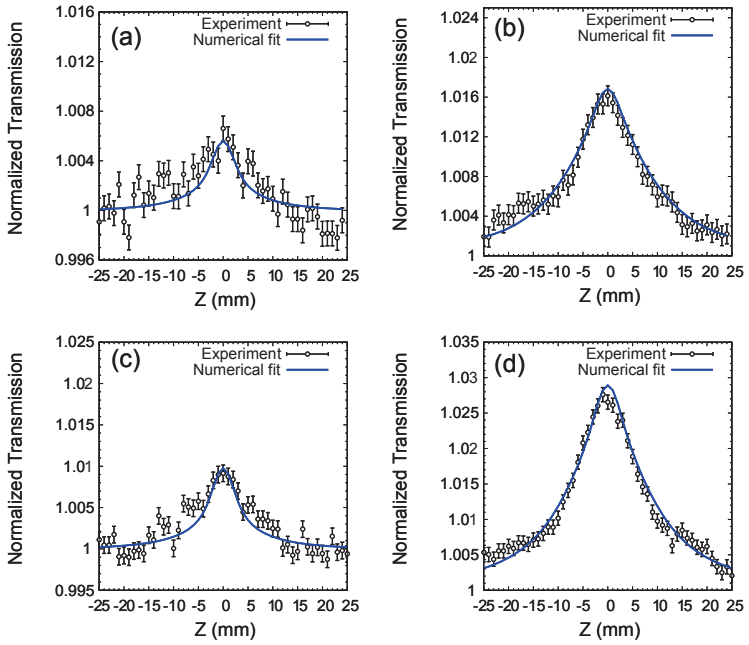

Fig. 6. Normalized transmission with respect to position of Cr^{4+}:YAG crystal (Z-scan curve). White circular symbols are experimentally measured results, and solid blue lines are numerically calculated results showing the best fit to the experimental plots. Z-scan curves of 1.3-mm-thick crystal measured with (a) 0.6 μJ and (b) 6.0 μJ pulses, and that of 2.4-mm-thick crystal measured with (c) 0.59 μJ and (d) 5.9 μJ pulses. The error-bars represent the uncertainty in the measurement mainly owing to the fluctuation of the Q-switched pulses.

In the numerical model to reproduce the Z-scan curves, the saturable absorption is described by the following three equations:

$$\frac{dI(r,t,z)}{dz} = -\sigma_{gs} n_{gs}(r,t,z) I(r,t,z) - \sigma_{es} n_{es}(r,t,z) I(r,t,z), \tag{7}$$

$$\frac{dn_{gs}(r,t,z)}{dt} = -\frac{\sigma_{gs} I(r,t,z)}{h\nu_L} n_{gs}(r,t,z) + \frac{n_{es}(r,t,z)}{\tau}, \tag{8}$$

$$\frac{dn_{es}(r,t,z)}{dt} = -\frac{dn_{gs}(r,t,z)}{dt}. \tag{9}$$

These rate equations have three variables: radial coordinate r, time t, and coordinate along the thickness of the crystal z. Coordinate z is zero at the incident surface and it varies up to l_{SA}, the thickness of the crystal. I is intensity, n_{gs} and n_{es} are density of ground- and excited-states, h is Planck's constant, and ν_L is laser frequency. Again, in the previous section, we proposed a model of a Cr^{4+}:YAG saturable absorber at 640-nm that has two separated excited-states; meanwhile the transition ratio γ was still unknown. However, we assumed here the transition ratio of $\gamma = 1$, because, in the next section, our rate equation analysis to reproduce a passively Q-switched Pr^{3+}:YLF laser indicates that fast recovery time must be dominant. Consequently, in this simulation, recovery time τ was assumed to 26 ns and the longer recovery time of 5.6 μs was neglected. The incident pulse was set to have a spatial and temporal Gaussian, and its

#240833 Received 15 May 2015; revised 30 Jun 2015; accepted 3 Jul 2015; published 17 Jul 2015

intensity distribution is written as follows:

$$I(r,t,z) = I_0 \exp\left\{-\left(\frac{2r^2}{w^2} + \frac{t^2}{t_p^2}\right)\right\}. \tag{10}$$

I_0 is the peak intensity of the incident pulse, w is beam radius ($1/e^2$) within the crystal, and t_p is pulse width (FWHM).

The waveform of the transmitted pulse was distorted owing to the nonlinear absorption of the saturable absorber, which was bleached by the forepart of the pulse. Therefore, the transmittance for the rear part of the pulse is higher than that for the forepart. The transmittance of the saturable absorber was measured as the ratio of energy of the transmitted pulse to that of the incident pulse. This can be described by the following equation:

$$T = \frac{\int_0^\infty F(r, l_{SA}) 2\pi r dr}{\int_0^\infty F(r,0) 2\pi r dr}. \tag{11}$$

Here, $F(r,z)$ is a pulse fluence given by $F(r,z) = \int_{-\infty}^{\infty} I(r,t,z)dt$. In the numerical simulation, this transmittance T was calculated for each position of the crystal Z with respect to the focal spot as the origin ($Z = 0$), varying from -25 to 25 mm. The ground- and excited-state absorption cross sections σ_{gs} and σ_{es} were determined by fitting a calculated Z-scan curve to an experimental Z-scan curve. The determined pair of σ_{gs} and σ_{es} simultaneously reproduced Z-scan curves with two different pulse energies. Solid lines in Fig. 6 are calculated Z-scan curves that minimize the difference with experimental plots based on the least square method. For the experiments with 1.3-mm-thick Cr^{4+}:YAG (Fig. 6(a) and 6(b)), calculated curves showed the best fit with $\sigma_{gs} = 1.70 \times 10^{-17}\text{cm}^2$ and $\sigma_{es} = 1.00 \times 10^{-17}\text{cm}^2$. For the experiments with 2.4-mm crystal (Fig. 6(c) and 6(d)), the numerical simulation showed best fit with $\sigma_{gs} = 1.75 \times 10^{-17}\text{cm}^2$ and $\sigma_{es} = 0.95 \times 10^{-17}\text{cm}^2$.

Once the absorption cross sections have been determined, we can estimate the total density of tetravalent chromium ions (Cr^{4+}), which contribute to the saturable absorption. Therefore, the estimated total density of Cr^{4+} which contributes the saturable absorption. n_{tot}, was $2.51 \times 10^{16}\text{cm}^{-3}$ and $2.06 \times 10^{16}\text{cm}^{-3}$ for 1.3-mm- and 2.4-mm-thick crystals, respectively. Although we obtained consistent values of absorption cross sections from the measurements with crystals of different thickness, the calculated total densities were different. This is probably because the

Table 1. Estimated parameters of 1.3-mm and 2.4-mm Cr^{4+}:YAG crystals.

l_{SA}(mm)	1.3	2.4
$\sigma_{gs}(\text{cm}^2)$	1.70×10^{-17}	1.75×10^{-17}
$\sigma_{es}(\text{cm}^2)$	1.00×10^{-17}	0.95×10^{-17}
$n_{tot}(\text{cm}^{-3})$	2.51×10^{16}	2.06×10^{16}
T_0 (%)	94.6	91.7
T_{sat} (%)	96.8	95.4
ΔT (%)	2.2	3.7

oxidization of Cr^{3+} ions is affected by the condition of fabrication, and it may be difficult to make Cr^{4+}:YAG crystals of the same concentration. A saturated transmittance T_{sat} is defined as the transmittance when the ground-state becomes empty, and it is theoretically given by the following equation:

$$T_{sat} = \exp(-\sigma_{es} n_{tot} l_{SA}). \tag{12}$$

#240833 Received 15 May 2015; revised 30 Jun 2015; accepted 3 Jul 2015; published 17 Jul 2015

According to this equation, the saturated transmittances of 1.3-mm and 2.4-mm Cr^{4+}:YAG crystals were calculated as 96.8 and 95.4%. These estimated parameters for the two crystals are summarized in Table 1.

3. Passively Q-switched Pr^{3+}:YLF laser at 640 nm and rate equation analysis

In this section, a Pr^{3+}:YLF laser passively Q-switched by a Cr^{4+}:YAG saturable absorber oscillating at 640 nm is presented. The set-up of the laser is depicted in Fig. 7. The V-fold laser cavity consists of three mirrors: a dichroic mirror (DM), a high-reflectivity (HR) concave mirror (CM) and a concave output coupler (OC) of 8.6%, with a curvature radius of 75 mm. The cavity length was approximately 22.5 cm. The angle of incidence on the CM was 11 degrees. The laser medium was a 0.5 at.% Pr^{3+}-doped YLF rod (Unioriental Inc.) whose diameter and length were both 5 mm, and its end surfaces were both uncoated. The laser crystal was mounted on a water-cooled copper holder to avoid a thermal load, which tends to fluctuate the laser output. The laser rod was pumped by polarization-combined InGaN blue LDs (Nichia Inc.). Each LD was mounted on a Peltier-cooled copper holder. The maximum output power of each LD was 3.5 W. The beam quality of the LD was $M^2 = 1.5 \times 12.9$ (fast × slow axes) calculated from its divergence angle and emitter size. The Pr^{3+}:YLF crystal has its absorption peaks at 444 nm and 442 nm for polarization parallel with the c-axis and a-axis of the crystal, respectively. Therefore, the temperatures of LD mounts were controlled to maximize the absorbed power.

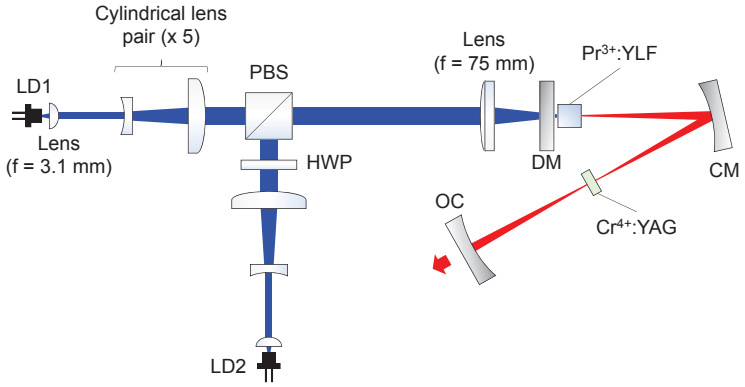

Fig. 7. Experimental set-up of an InGaN blue LD pumped Pr^{3+}:YLF laser passively Q-switched by a Cr^{4+}:YAG saturable absorber oscillating at 640 nm. PBS: polarization beam splitter, HWP: half wave plate, DM: dichroic mirror, CM: concave mirror, OC: output coupler.

Both pump beams were collimated by an aspherical lens of 3.1-mm focal length, and expanded along the slow axis of the LD by a pair of cylindrical lenses by a factor of five. Then, these beams were combined by a polarization beam splitter, and focused into the laser rod by a lens of 75-mm focal length. The pump spot size within the gain medium was calculated to be 5.6 × 33 μm. A Cr^{4+}:YAG saturable absorber of 1.3-mm or 2.4-mm length characterized in the previous section was inserted into the focal spot between CM and OC. The Cr^{4+}:YAG crystal was not temperature-controlled. The beam width inside the cavity was calculated by means of the ABCD matrix method, and the maximum mode-matching efficiency was calculated to be 78%. Before the Q-switching experiment, we performed a CW operation by simply removing the Cr^{4+}:YAG from the cavity. Its maximum output power reached 1.52 W with a maximum absorbed pump power of 4.3 W, and the slope efficiency was 43.7%. The threshold pump

#240833 Received 15 May 2015; revised 30 Jun 2015; accepted 3 Jul 2015; published 17 Jul 2015

power was 770 mW. With the maximum output, the beam quality factor was measured to be $M^2 = 1.1 \times 1.7$ along the fast and slow axes, respectively.

Subsequently, we performed Q-switching using a Cr^{4+}:YAG saturable absorber of 1.3-mm and 2.4-mm length. The experimental output power with respect to the absorbed pump power is shown as solid lines with circular plots in Fig. 8.

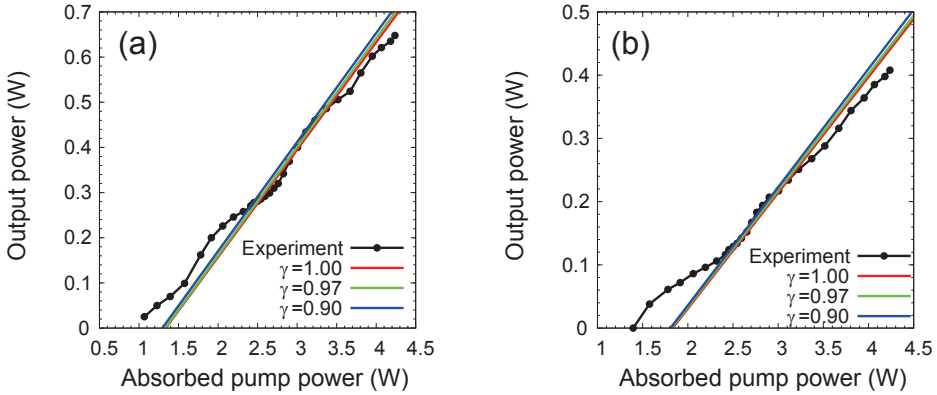

Fig. 8. Output characteristics of the passively Q-switched laser with a (a) 1.3-mm- and (b) 2.4-mm-long Cr^{4+}:YAG crystal. Black solid-lines with circular plots are experimental results, and three colored lines correspond to calculated results with different transition ratios γ to the excited-state, which has a lifetime of 26 ns.

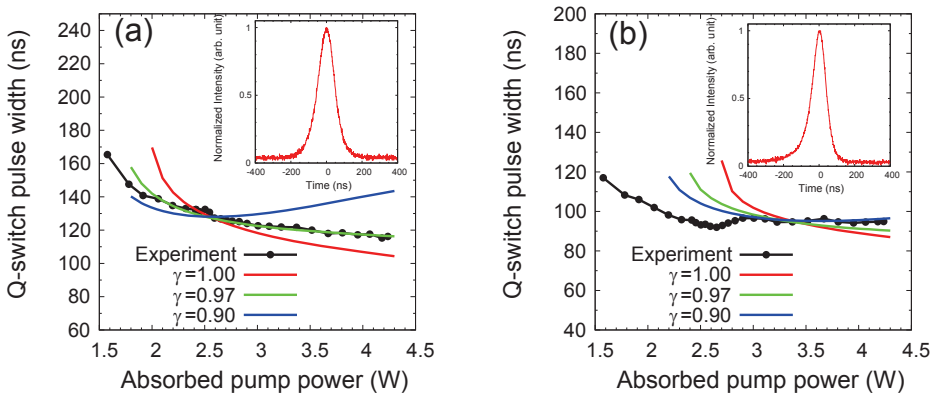

Fig. 9. Q-switch pulse width (FWHM) of the Q-switched laser with a (a) 1.3-mm- and (b) 2.4-mm-long Cr^{4+}:YAG crystal with respect to the absorbed pump power. Three colored lines are calculated results with different transition ratios γ. The insets are pulse waveformes recorded with maximum absorbed pump power.

The maximum output power and slope efficiency with the 1.3-mm and 2.4-mm saturable absorbers reached 0.65 W and 0.41 W, and 20.2% and 14.6%, respectively. Although the output beam was not fundamental mode in CW operation, the measured beam quality of the Q-switched laser was nearly fundamental mode ($M^2 < 1.1$) because the higher cavity modes underwent lower transmission of the saturable absorber. The measured Q-switched pulse width

#240833 Received 15 May 2015; revised 30 Jun 2015; accepted 3 Jul 2015; published 17 Jul 2015

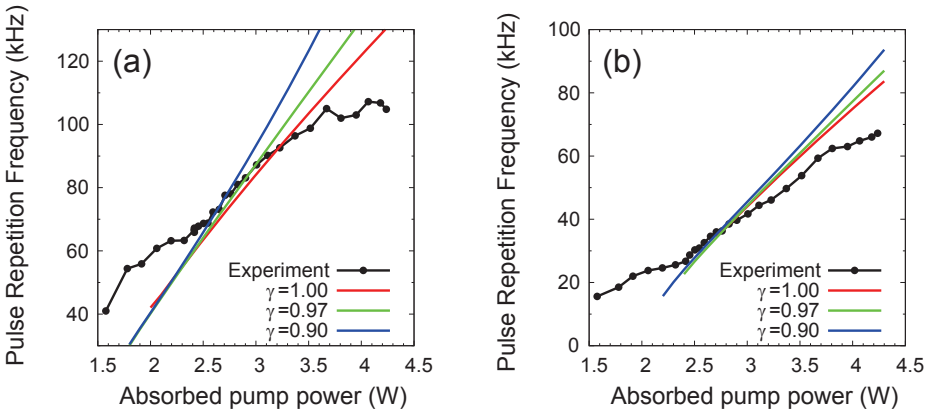

Fig. 10. Pulse repetition frequency of the Q-switched laser with a (a) 1.3-mm- and (b) 2.4-mm-long Cr^{4+}:YAG crystal with respect to the absorbed pump power. Three colored lines are calculated results with different transition ratios γ.

with respect to the absorbed pump power is shown as solid lines with circular symbols in Fig. 9. The pulse width with a 1.3-mm- and 2.4-mm-long Cr^{4+}:YAG converged around 120 and 95 ns. It is consistent that the pulse width with the thicker saturable absorber got shorter because of its larger modulation depth. The pulse waveforms were recorded by a 1-GHz photodiode (Hamamatsu, Si PIN photodiode S3883) with maximum absorbed pump power, and shown as the insets of the figures. The pulse repetition frequency is shown as solid lines with circular symbols in Fig. 10. The repetition rate increased monotonically with the absorbed pump power. With the maximum output power, the highest pulse repetition rates were 105 and 67 kHz for Q-switched laser with the 1.3-mm and 2.4-mm Cr^{4+}:YAG, respectively. The highest pulse energy and peak power were therefore calculated to be 6.2 μJ and 53.2 W with the 1.3 mm crystal, and 6.1 μJ and 64.0 W with the 2.4 mm crystal.

To check the accuracy of the model and estimated parameters of the Cr^{4+}:YAG saturable absorbers listed in Table 1, we numerically solved the following rate equations representing a passively Q-switched laser, and compared them with the experimental results, in the same manner as that reported by Kojou *et al.* [9]:

$$\frac{d\phi}{dt} = \frac{c\phi}{l_c}\left\{\sigma_{st}Nl_g - \sigma_{gs}n_g l_{SA} - \sigma_{es}n_{es1}l_{SA} - \sigma_{es}\left(n_{tot} - n_g - n_{es1}\right)l_{SA}\right\} - \frac{\phi}{\tau_c} + \frac{\xi N}{\tau_f}, \tag{13}$$

$$\frac{dN}{dt} = -c\phi\sigma_{st}N - \frac{N}{\tau_f} + \frac{N_{tot} - N}{N_{tot}}\frac{\eta P_{abs}}{h\nu_L V}, \tag{14}$$

$$\frac{dn_g}{dt} = -\sigma_{gs}c\phi n_g A_g/A_{SA} + \frac{n_{es1}}{\tau_1} + \frac{n_{tot} - n_g - n_{es1}}{\tau_2}, \tag{15}$$

$$\frac{dn_{es1}}{dt} = \gamma\sigma_{gs}c\phi n_g A_g/A_{SA} - \frac{n_{es1}}{\tau_1}. \tag{16}$$

The model consists of rates of four parameters: photon density ϕ, population inversion N, population density of the ground-state in the saturable absorber n_g, and in the first excited-state n_{es1}, which has the lifetime τ_1. c is speed of light. σ_{st} is the stimulated emission cross section of the gain medium. l_g is the length of the laser rod. σ_{gs} and σ_{es} are the ground- and excited-state absorption cross sections of the saturable absorber. l_{SA} is the length of the saturable absorber. The population density of the second excited-state in the saturable absorber n_{es2}, whose life-

#240833 Received 15 May 2015; revised 30 Jun 2015; accepted 3 Jul 2015; published 17 Jul 2015

time is τ_2, is given as $n_{tot} - n_g - n_{es1}$ because the lifetimes of other states (E_3, E_4 and E_6 in Fig. 4) are assumed to be very fast. l_c is the cavity length. τ_c is photon lifetime in the cavity defined as $2l_c/c(L_i - \ln R)$, where L_i and R are the round-trip loss of the cavity, and the reflectivity of the output coupler, respectively. ξ is the rate at which spontaneous emission is added to the laser emission. τ_f is the fluorescent lifetime of the gain medium, and therefore, N/τ_f stands for the rate of spontaneous emission. N_{tot} is the total population density of the active ions in the gain medium. η denotes the total efficiency of the laser including quantum, pump, and mode-matching efficiencies. P_{abs} is the pump power absorbed by the gain. V is the mode volume. A_g and A_{SA} are effective mode cross sections in the gain medium and the saturable absorber, respectively. While we adopted the simple plane wave approximation, we separately calculated the mode volume and mode matching efficiency using the spatial beam profile of the pump beam and cavity mode in our experiment. Once the mode size and mode matching efficiency were calculated, the simple plane wave rate equation model is adequate to describe the laser performance.

During our analysis of Cr^{4+}:YAG saturable absorption, the transition ratio γ was still unknown while the absorption cross sections have been estimated. Therefore, we numerically solved these rate equations by varying γ. The calculated results are shown in Figs. [8-10], as colored lines. The rate equation analysis indicated that only Q-switched pulse width is strongly affected by the transition ratio γ, and the experimentally obtained pulse width cannot be reproduced when γ is small. According to the rate equation analysis, the pulse width would increase as the absorbed pump power increased if the transition ratio γ was smaller than 0.95. We numerically simulated the temporal transmission of a probe laser through a Cr^{4+}:YAG crystal in the pump-probe experiment (Fig. 2) with the transition ratio γ of 0.95, and the calculated result showed good agreement with the result of the pump-probe measurement presented in Fig. 3(b). We can consequently suppose that the Q-switching action was mainly dominated by the shorter recovery time τ_1 , which had been estimated to be 26 ns. Although the longer recovery time τ_2 is not dominant, it enabled us to explain the convergence of the pulse width with higher absorber pump power. Furthermore, we could check the accuracy of the absorption cross sections of the Cr^{4+}:YAG crystals by the fact that the calculated results successfully reproduced the Q-switched pulse width, which is strongly influenced by the modulation depth of the saturable absorber. As shown in Fig. 10, the experimental slope in the pulse repetition frequency is lower than that of the model calculation. In passively Q-switched lasers, the pulse repetition rate is proportional to its averaged output power, because once the lasing starts, the pulse energy no longer changes with the pump power. Therefore, the experimental slope efficiency in Fig. 8 is also slightly lower than that of our model calculation.Presumably our mode matching efficiency was slightly underestimated, but we did not treat the mode matching efficiency as another adjusting parameter because we placed an emphasis on the discussion of the saturable absorption of the Cr^{4+}:YAG in this paper.

4. Design of Pr^{3+}:YLF microchip laser Q-switched by Cr^{4+}:YAG saturable absorber

The duration of pulses generated by Q-switching strongly depends on the cavity length, and the shortening of the laser cavity is an effective way to make pulse duration shorter. The shortening of the pulse enables us to achieve a higher peak power. In this section, we therefore present a design of a Pr^{3+}:YLF microchip laser Q-switched by a Cr^{4+}:YAG saturable absorber oscillating at 640 nm, and its predicted performance. By using the parameters of the saturable absorber and the rate equations, we can now simulate the microchip laser.

Although Nd:YAG microchip lasers adopted a plane-plane cavity stabilized by a thermal lens of positive focal length appearing in the laser rod, we adopted a conventional plane-concave cavity, since the YLF crystal tends not to form a thermal lens owing to its negative thermo-

#240833 Received 15 May 2015; revised 30 Jun 2015; accepted 3 Jul 2015; published 17 Jul 2015

optical coefficient (dn/dt) [23]. A concave-plane cavity of 2-cm length, composed of an HR concave mirror of 2-cm curvature radius and a plane output coupler of 20% transmission, is assumed. We set the maximum absorbed pump power of 6 W, which can be achieved by the polarization-combined blue LD pair as in Fig. 7. As a gain medium, a 3-mm-long Pr^{3+}:YLF crystal of 1 at.% dope concentration is assumed. Richter investigated the fluorescence quenching effect of the Pr^{3+}:YLF crystal [24], and according to the report, the effective fluorescence lifetime of a 1 at.% doped Pr^{3+}:YLF crystal is approximately 28 μs. The modulation depth of the saturable absorber affects the pulse width and pulse energy. The pulse energy increases and the pulse width is shortened as the modulation depth increases. However, the large modulation depth simultaneously brings a large non-saturable loss. Here, we set the initial transmission and the modulation depth of the Cr^{4+}:YAG saturable absorber to be 70 and 12.4%, which are calculated based on Eqs. (4)(12) with $\sigma_{gs} = 1.70 \times 10^{-17}\text{cm}^2$ and $\sigma_{es} = 1.00 \times 10^{-17}\text{cm}^2$. The transition ratio γ was set to be 0.95.

The rate equation calculation predicted the averaged output power of 600 mW, the pulse width of 860 ps, the pulse energy of 11.3 μJ, and the peak power of 13.1 kW with an absorbed pump power of 6 W. The pulse energy and the peak power can be further increased by employing a Cr^{4+}:YAG saturable absorber of larger modulation depth. From these sample calculations, we may obtain subnanosecond red laser pulses from compact solid-state laser devices.

5. Conclusion

In this paper, we reported the characterization of a Cr^{4+}:YAG saturable absorber at 640 nm for the first time, by means of pump-probe and Z-scan experiments. The pump-probe measurement revealed that the Cr^{4+}:YAG has two absorption recovery times, which were estimated to be 26 ns and 5.6 μs. We subsequently evaluated the ground- and excited-state absorption cross sections by Z-scan measurement and the numerical simulation based on the rate equation calculation, and these cross sections were estimated to be $1.70 - 1.75 \times 10^{-17}\text{cm}^2$ and $0.95 - 1.00 \times 10^{-17}\text{cm}^2$, respectively. Furthermore, we demonstrated an InGaN blue LD pumped passively Q-switched Pr^{3+}:YLF laser using a Cr^{4+}:YAG as the saturable absorber. With the maximum absorbed pump power of 4.3 W, we obtained the averaged output powers of 0.65 and 0.41, the slope efficiencies of 20.2 and 14.6%, and the Q-switched pulse widths of 115 and 95 ns by employing Cr^{4+}:YAG crystals 1.3- and 2.4-mm-long, respectively. The calculated highest pulse energies were 6.2 and 6.1 μJ, and the highest peak powers were 53.2 and 64.0 W with each crystal. To confirm the accuracy of the characterization of the Cr^{4+}:YAG, we numerically solved rate equations representing the Q-switched laser with the experimentally estimated parameters. The calculated results showed good agreement with the experimental results, and the calculated Q-switched pulse width revealed that the shorter absorption recovery time was dominant for Q-switching. We designed a passive Q-switching laser and anticipated its performance from rate equation simulation with the estimated parameters of Cr^{4+}:YAG at 640 nm. A numerical simulation revealed that a microchip passive Q-switching Pr^{3+}:YLF laser is able to generate subnanosecond pulses, and a 10-kW peak power can be achieved.

Acknowledgments

We gratefully thank Nichia Inc. for supplying the high-power InGaN blue laser diodes. This research was supported by a Grant-in-aid from the Ministry of Education, Culture, Sports, Science, and Technology, Japan for the Photon Frontier Network Program and by JSPS KAKENHI Grant Number 24656055. This work was also supported in part by a Grant-in-Aid for the Program of Leading Graduate Schools of Keio University for "Science for Development of Super Mature Society" from the Ministry of Education, Culture, Sport, Science, and Technology in Japan.

#240833 Received 15 May 2015; revised 30 Jun 2015; accepted 3 Jul 2015; published 17 Jul 2015